Investigation of structural and electrical characteristics of PZT ceramics modified with donor and acceptor dopants

M. N. Al-Aaraji[1]*, A. H. Uqla[1]

[1]Department of Ceramic Engineering and Building Materials, College of Materials Engineering, University of Babylon, Al Hilla, Iraq

Abstract

Lead-based (PZT) ferroelectric ceramic materials were prepared utilizing the solid-state reaction method as a pure and doped with different additives. As a pure form, the composition with the chemical formula $Pb_{1.03}(Zr_{0.56}Ti_{0.44})O_3$ characterized as rhombohedral structure according to the PZT phase diagram region was investigated systematically. Different strategies of doping were followed to investigate the influence of donor and acceptor ions in addition to complex doping on structural and microstructure properties of the parent composition: for the soft ceramic, 2 mol% lanthanum-doped PZT at A-site (PLZT), whereas 2 mol% of scandium-doped PZT at B-site to produce hard ceramic (PSZT). In terms of complex doping, 2 mol% of both La^{3+} and Sc^{3+} substituted A- and B-site, respectively (PLSZT). All samples showed dense and homogeneous microstructures, except PSZT ceramic displayed a small grain size. X-ray diffraction results showed that the addition of Sc^{3+} induced phase transformation and formation of a coexistence region consisting of tetragonal and rhombohedral phases. This region was recognized in both PSZT and PLSZT compositions. Hard ceramic (Sc^{3+}-doped PZT) exhibited the highest values of relative permittivity and lowest dielectric loss at a frequency of 100 kHz.
Keywords: lead-based ceramics, ferroelectrics, phase transformation, dielectrics.

INTRODUCTION

Ferroelectricity in polycrystalline ceramics (like barium titanate, $BaTiO_3$) was discovered in the 1940s, followed by a continuous succession in exploring characteristic features of ferroelectrics and related materials including piezoelectrics and pyroelectrics [1]. Ferroelectric materials exhibit several useful features, such as high piezoelectric responses, including switchable polarization, and high dielectric constants. As a result, they are widely utilized in a variety of devices such as ultrasonic generators, memory elements, gas igniters, capacitors, and many more. Lead zirconate titanate $Pb(Zr_xTi_{1-x})O_3$ is a unique example of a ferroelectric material that has been widely investigated in the previous decade as one of the most attractive ferroelectric materials with high Curie temperature (T_c). PZTs have a diverse set of features that make them appealing candidates for sensing applications and a wide range of microelectronics [2, 3]. Because of its excellent dielectric and piezoelectric characteristics, $PbZrO_3$-$PbTiO_3$ solid solution, abbreviated as PZT, has dominated economically for several decades. Because of its high piezoelectric response, PZT has become one of the most widely used materials for electromechanical applications [4]. This wide variety of functional characteristics may be attained by modifying the Zr/Ti ratio and using minor dopants based on the application requirements. Doped PZT ceramics are primarily classified as 'soft' or 'hard', and are typically made by replacing the A-site ions with donor dopants or B-site ions with acceptor ones [5]. Hard PZT exhibits high piezoelectric coefficients, lower permittivity, low dielectric loss, elastic compliances, noticeable aging, mechanical losses, decreased resistivity, and pinched ferroelectric hysteresis in the old state as compared to the undoped composition. In contrast, soft PZT has better characteristics, bigger losses, enhanced resistivity, less aging, square polarization loops, and simple poling and depoling [6].

Intensive studies were conducted with different strategies and types of doping of PZT materials. For instance, La^{3+}-doped PZT ceramic as a donor at A-site is reported widely as a relaxor or antiferroelectric materials to be used in energy-storage applications [7-9]. It was found that this substitution causes lattice distortion which enhances the tetragonality of the PLZT unit cell. As a result, it improves spontaneous polarization [10]. In this regard, it is reported previously that the addition of 2% La^{3+} as a donor at the A-site of PZT composition at the rhombohedral region enhances the tetragonality of the resulting PLZT unit cell without causing phase transformation [11]. In addition, it is found that this additive results in a reduction in the grain size. In terms of ferroelectric responses, it is reported that doping with lanthanum improves the domain switching which results in a rectangular polarization-electric field (P-E) hysteresis loop. Caceres et al. [12] investigated the effect of erbium Er^{3+} on the electrical properties of PZT and discovered that Er^{3+} caused the sample's density to rise ($91.9\% < \varrho < 99.0\%$) when compared to an undoped sample. In addition, the X-ray diffraction (XRD) pattern corresponding to the tetragonal crystalline structure was observed. For acceptor doping, Sangawar et al. [13] studied the effect of Fe on lead zirconate titanate ceramics. It is reported that the tetragonal

**mohammed.al_aaraji@uobabylon.edu.iq*
https://orcid.org/0000-0001-7261-4595

splitting in PZT rises as the Fe level increases. Also, Mahato et al. [14] investigated the effect of doping lead zirconate titanate (PZT) ceramics with Na dopants. It is clear that the shape of the grains changes and their size also decreases with incorporation of Na^+ substituents. It was found that the coercive field (E_c) can decrease by substitution with an acceptor dopant; for example, Sc^{3+} when replacing the B-site cation of PZT. As well as it was reported that doping with Sc can develop relaxor behaviors in several perovskites such as $Pb_{0.78}Ba_{0.22}Sc_{0.5}Ta_{0.5}O_3$ [15] and $PbSc_{0.5}Nb_{(1-x)/2}Ta_{x/2}O_3$ (PSNT) with $0 \leq x \leq 1$ [16].

In terms of co-doping in PZT ceramics, Zak et al. [4] investigated the influence of Y^{3+} and Nb^{5+} co-doping on the piezoelectric and dielectric characteristics of $Pb_{1-x}Y_x(Zr_{0.53}Ti_{0.47})_{1-x}Nb_xO_3$ ceramics. It is found that the tetragonality rises at doping levels x= 0.01 and 0.03. Scanning electron microscopy (SEM) results showed that the average grain size of doped PZT is around 3 μm, which is smaller than that of pure PZT. Recently, Bhattarai et al. [17] studied the influence of La^{3+} and Sc^{3+} content on the structural, ferroelectric, and dielectric properties of lead zirconate titanate ceramics for energy storage capacitors, as complex doping, with the stoichiometric formula $(PbZr_{0.53}Ti_{0.47})_{0.90}(La_xSc_{1-x})_{0.10}O_3$ for x= 0.2, 0.4, 0.6, and 0.8. The higher content of La^{3+} composition showed relaxor behavior. The P-E loop measurements in the specimen with composition at x=8 demonstrated that there is an enhanced P_m-P_r (maximum polarization-remanent polarization), which results in a recoverable energy density, U_{re} ~1162 J/cm^3 with an efficiency η of ~79% under an applied electric field of ~97 kV/cm, and, therefore, it can be a promising material for energy-storage applications. The coercive field (E_c) was found to decrease upon increasing La^{3+} concentration; the highest field E_c was observed for a low La^{3+} content. This is in accordance with that of a report on Sc^{3+}-doped $PbZr_{0.53}Ti_{0.47}O_3$, wherein no substantial reduction in E_c was observed [18]. They also noticed that upon increasing the lanthanum content, the spontaneous polarization (P_m) first increases, peaks at composition x=6 with Pm ~35 μC/cm^2, and then decreases. The observed slim hysteresis loop and higher differences in the P_m-P_r value for the sample with composition at x=8 suggest that this composition is a relaxor in nature [17].

The main goal of this project was to obtain optimized PZT ceramics around the morphotropic phase boundary (MPB) region in terms of structural and electrical properties throughout doping. For this purpose, we propose that the doping in PZT composition close to the MPB region could help to cause a phase transformation that can be employed in different applications. Therefore, the dopant ions substitute the Zr^{4+} and Pb^{2+} sites. It is expected that single or co-substitution of Sc^{3+} and La^{3+} at these sites could induce relaxor ferroelectrics characteristics, which results in an improved slim P-E loop and consequently improve its storage energy behavior. The prepared undoped and doped samples were characterized using XRD and SEM techniques to characterize the parent composition and to investigate the influence of doping ions on the structure and microstructure properties. Furthermore, functional characterization of the produced ceramics should be achieved, including relative permittivity, dielectric breakdown, and conductivity to evaluate the possibility of using them in electrical applications.

EXPERIMENTAL PROCEDURES

Based on the aforementioned information, PZT composition at Zr/Ti ratio equal to 0.56/0.44 was chosen according to the formula $Pb(Zr_{1-x}Ti_x)O_3$ which is located at the rhombohedral region. The dopants ions La^{3+} and Sc^{3+} are expected to substitute the Pb^{2+} and Zr^{4+} sites, respectively. More precisely, the parent PZT composition was doped with 2% lanthanum (La^{3+}) as a donor dopant at the A-site $(Pb_{0.98}La_{0.02})(Zr_{0.56}Ti_{0.44})O_3$ (PLZT) and 2% scandium (Sc^{3+}) as an acceptor dopant at the B-site $Pb(Sc_{0.02}Zr_{0.54}Ti_{0.44})O_3$ (PSZT); furthermore, it was also co-doped with 2% lanthanum and 2% scandium $(Pb_{0.98}La_{0.02})(Sc_{0.02}Zr_{0.54}Ti_{0.44})O_3$ (PLSZT). Undoped and doped ceramics were prepared by conventional solid-state reaction method using high purity powders of PbO (Sigma Aldrich, 99% purity), La_2O_3 (Alfa Aesar, 99.9% purity), ZrO_2 (E-101, Magnesium Elektron), TiO_2 (A-HR, Huntersman, 99% purity), and Sc_2O_3 (Sigma Aldrich, 99% purity).

Starting powders were weighed according to the molar ratios of the chosen composition, with an excess of 0.03 mol% of PbO. For a typical milling process, 20 g of powder was mixed with 20 g zirconia balls (7.0 mm in diameter) as milling media were put together inside a polyethylene bottle and wet-milled using 25 mL isopropanol. Then, the mixture was placed in a roller-milling machine for 15 h. The obtained slurry was then dried at 90 °C. Afterward, a high-density alumina crucible covered with an alumina plate was used to calcine dry particles. The powders were calcined for 3 h at 800 °C with a heating rate of 10 °C/min. Calcined powders were wet milled for 15 h in a manner similar to the original milling to promote agglomeration size reduction. Regarding the production of bulk samples as pellets for various tests, 2 wt% of polyethylene glycol (PEG) was utilized as a binder in a water solution to increase the plasticity of the powders. Powders and PEG solutions were combined, dried, and then milled using zirconia balls in a roller milling machine. The dry powder, including the binder, was pressed uniaxially into pellets in a cylindrical stainless-steel die for 40 s at a pressure of 150 MPa. These pellets were 10 mm in diameter and 0.9 to 1.2 mm in thickness, depending on the electrical measurement's requirements. To prevent severe evaporation of the lead during sintering, pellets were put on a thin layer of zirconia sand (baddeleyite sand) and covered with an alumina crucible in the presence of $PbZrO_3$ powder. The sintering process was conducted in two steps. First, the samples were heated up to 500 °C with a heating rate of 5 °C/min and soaked for 30 min to guarantee complete binder removal. After that, the samples were heated up to 1250 °C at a rate of 10 °C/min and kept for 2 h as a dwell period.

In terms of physical properties, the Archimedes method

was utilized to measure the bulk densities of the prepared ceramics using water as the immersion medium. Phase analysis was conducted by X-ray diffraction (XRD) using a diffractometer (XRD 6000, Shimadzu) with CuKα radiation having a wavelength of 1.54060 Å. Before analysis, the pellets were crushed into fine powders, and the measurement was achieved at room temperature with a step size of 0.02°, a speed of 6 °/min, and the detection range was 20° to 60°. The peak positions of the data were compared to the information from the JCPDS files in order to determine the presence of the perovskite structure and other phases. The microstructural features of polished and gold-coated surfaces of the prepared ceramics were characterized by scanning electron microscopy (VEGA3, Tescan). Electrical measurements including relative permittivity, loss tangent, and electrical conductivity were conducted using an LCR meter in the range of 100-1000 kHz at room temperature, whereas dielectric strength was determined by a high voltage supplier (PGO S3, Baur).

RESULTS AND DISCUSSION

Structure and microstructure properties

Structure characterization: the XRD patterns at room temperature for sintered undoped and doped PZT are shown in Fig. 1. Generally, peaks were sharper (in comparison with that of calcined powder) in agreement with a better crystallization or compositional homogenization due to high sintering temperatures. No peaks associated with the second-phases were observed. For the undoped composition (Fig. 1a), the single (200), as well as the little split (111) peaks, indicated that the ceramic had a rhombohedral structure, which was consistent with previous reports [11]. For soft ceramic, labeled PLZT, the influence of incorporation of 2 mol% of lanthanum on the crystal structure of PZT is illustrated in Fig. 1b. It was evident that there was no pronounced effect, albeit it could be seen a broadening in the (200) peak. On the other hand, Fig. 1c clearly shows the XRD pattern of hard PSZT that represented the incorporation of 2 mol% of scandium at the B-site (on account of the Zr ratio). As a perusal of the data, it was seen that the addition of Sc^{3+} induced partial phase transformation which resulted in the appearance of a tetragonal phase beside the rhombohedral phase. This can be well distinguished from the scanning patterns at around 2θ ~44°, where two overlapping diffraction peaks at the shoulders of (200) peak were observed. These can be ascribed to the development of the tetragonal phase. However, the relatively small peak splitting in those planes and the splitting of the (111) peak indicated a high fraction of the rhombohedral phase. As a result, this created a phase coexistence region (i.e., MPB region) which was consistent with the fact that the compositions were near the MPB. Fig. 1d shows the effect of complex doping on the structure of PZT, in which 2 mol% of both La^{3+} and Sc^{3+} were incorporated at the A- and B-site, respectively. Clearly, it was noticed strong peak splitting in the (200) plane, which suggested the increase of the ferroelectric tetragonal phase in comparison with hard PZT (PSZT). Furthermore, with the presence of La^{3+}, it was evident that the tetragonality or the

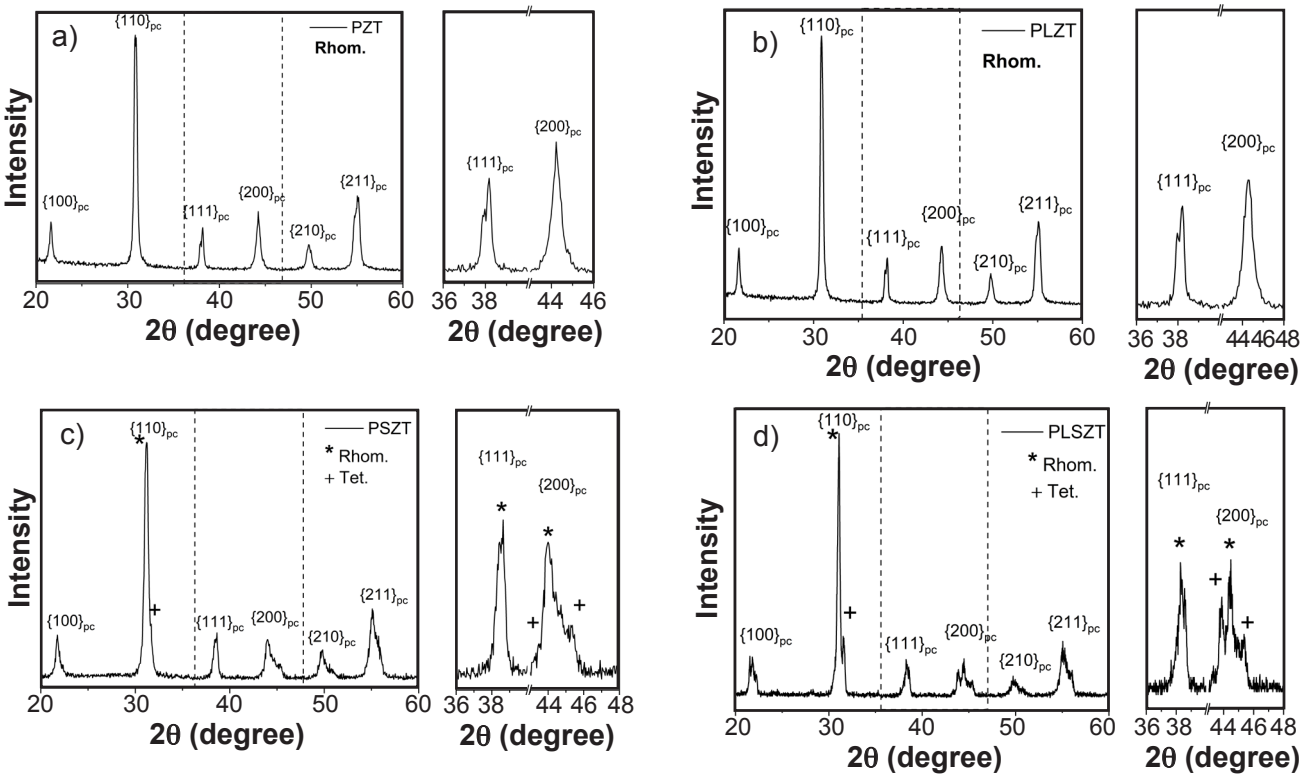

Figure 1: XRD patterns of ceramics sintered at 1250 °C for 2 h: a) PZT; b) PLZT; c) PSZT; and d) PLSZT.

lattice distortion along the tetragonal c-axis was decreased after doping, as evidenced by changes in the locations of the $(200)_{pc}$ and $(002)_{pc}$ diffraction peaks. This was directly related to the spontaneous strain (i.e., the c/a ratio was reduced for the La-doped PZT). This was attributed to the differences in the ionic size of Pb^{2+} and La^{3+}, which are 1.20 and 1.15 Å, respectively, and to the less distorted bonding arrangement of the La^{3+} ions.

Table I - Compositional formulas and physical properties of the PZT ceramics.

Composition	Code	Density ($g.cm^{-3}$)	Mean grain size (μm)
$Pb_{1.03}(Zr_{0.56}Ti_{0.44})O_3$	PZT	7.74	7.72
$Pb_{1.01}La_{0.02}(Zr_{0.56}Ti_{0.44})O_3$	PLZT	7.70	3.20
$Pb_{1.01}(Sc_{0.02}Zr_{0.54}Ti_{0.44})O_3$	PSZT	7.20	0.50
$(Pb_{1.01}La_{0.02})(Sc_{0.02}Zr_{0.54}Ti_{0.44})O_3$	PLSZT	7.60	3.85

Density and microstructure: the selected compositions of undoped and doped PZT ceramics with their formulas are illustrated in Table I. In addition, a summary of their

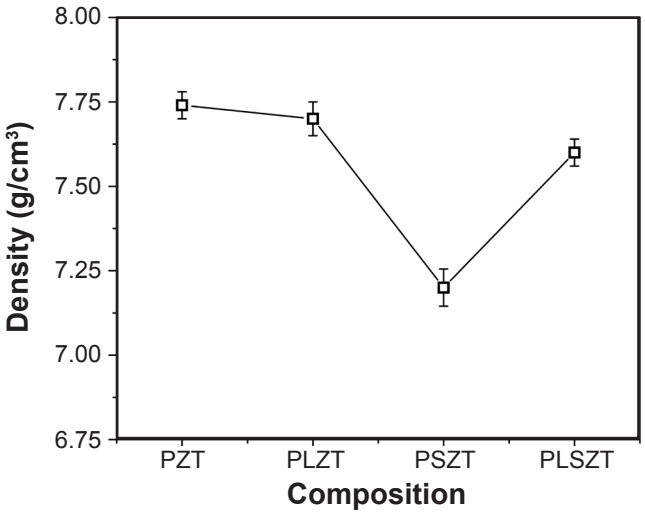

Figure 2: Bulk density of undoped and doped ceramics sintered at 1250 °C for 2 h.

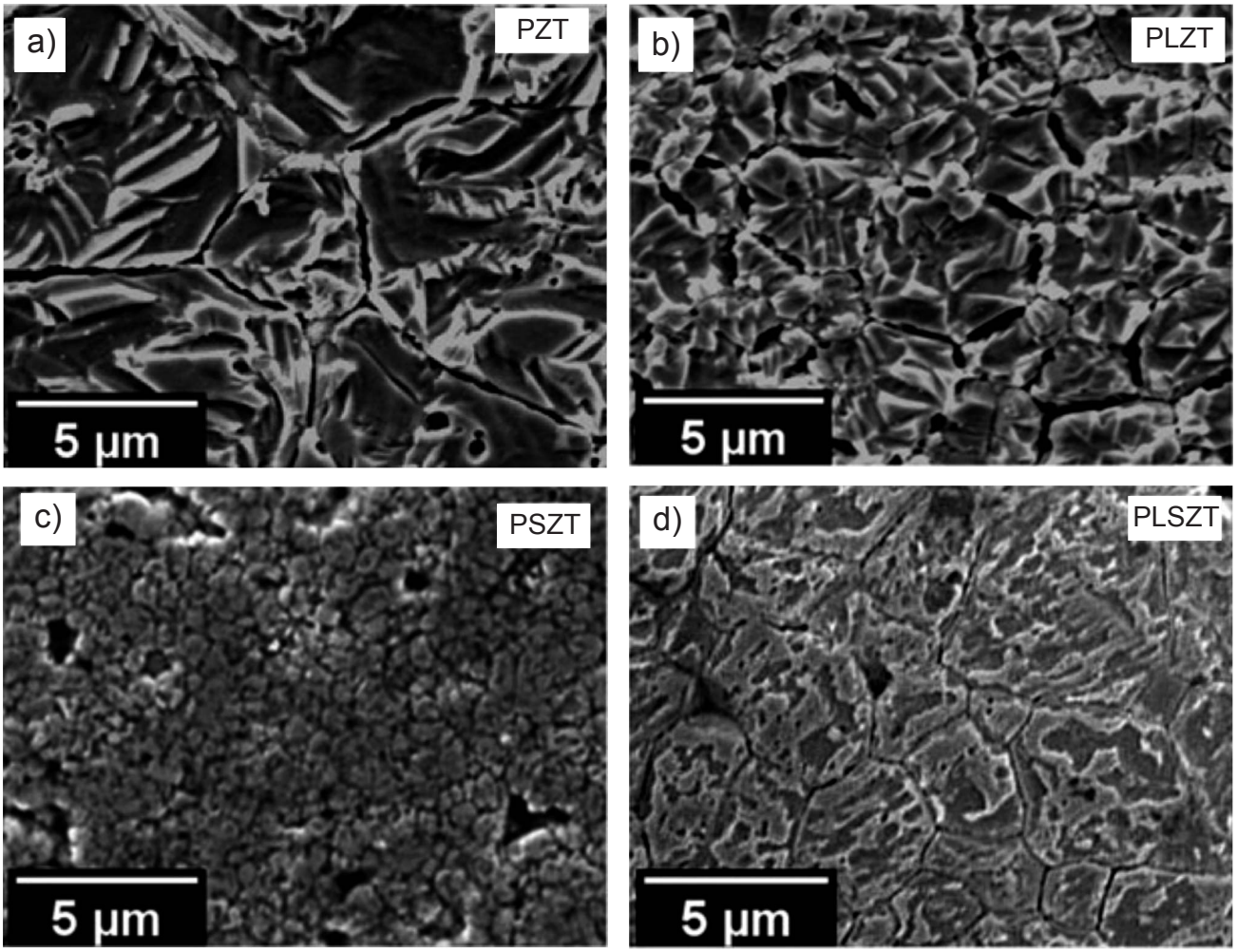

Figure 3: SEM micrographs of surface morphology of polished and chemically etched surfaces of undoped and doped PZT ceramics: a) undoped PZT; b) La-doped PZT; c) Sc-doped PZT; and d) La-Sc-doped PZT.

densities and mean grain sizes are listed and also shown in Fig. 2. In general, only the hard ceramic (PSZT) exhibited low density around ~7.2 g.cm^{-3}. Other ceramics possessed high values of density after sintering, greater than 95% of the theoretical density (assuming that the theoretical density was ~8.07 g.cm^{-3}). After doping with 2 mol% of La^{3+}, it was observed that the densities slightly decreased after doping as shown in Fig. 2. This observation was consistent with the finding of Pdungsap et al. [19], who reported that the density of PZT (52/48) decreased slightly with increasing lanthanum content.

Fig. 3 shows SEM micrographs of the surface morphology of polished and chemically etched surfaces of undoped and doped PZT ceramics. The samples were over-etched chemically. Therefore, it can be seen distorted surfaces that exhibited lots of pits. Generally, they revealed dense and homogeneous microstructures except for the PSZT which exhibited small grain size and relatively higher porosity. The mean grain size values of the ceramics are listed in Table I. They were measured from the SEM images with a scale of 20 μm using the linear intercept method. A comparison of the SEM images obtained for PZT and PLZT ceramics displayed that the average grain sizes of the PZT ceramics were reduced to less than half after doping with La. This observation supported the results of the earlier studies in which the grain size decreased sharply from ~7 μm to even lower than ~3 μm when PZT ceramics were doped with 2 at% La [20]. Langman et al. [21] assigned this grain size reduction to the solid solution impurity drag mechanism, which considers that the presence of the La^{3+} ion concentration gradient at grain boundaries causes the blocking of grain boundary mobility and subsequently leads to slower grain growth.

Electrical properties

Relative permittivity and dielectric loss: Fig. 4 shows the frequency-dependence of dielectric loss and relative permittivity (ε_r) of soft and hard ceramics in the range between 100 and 1000 kHz, at room temperature. Overall,

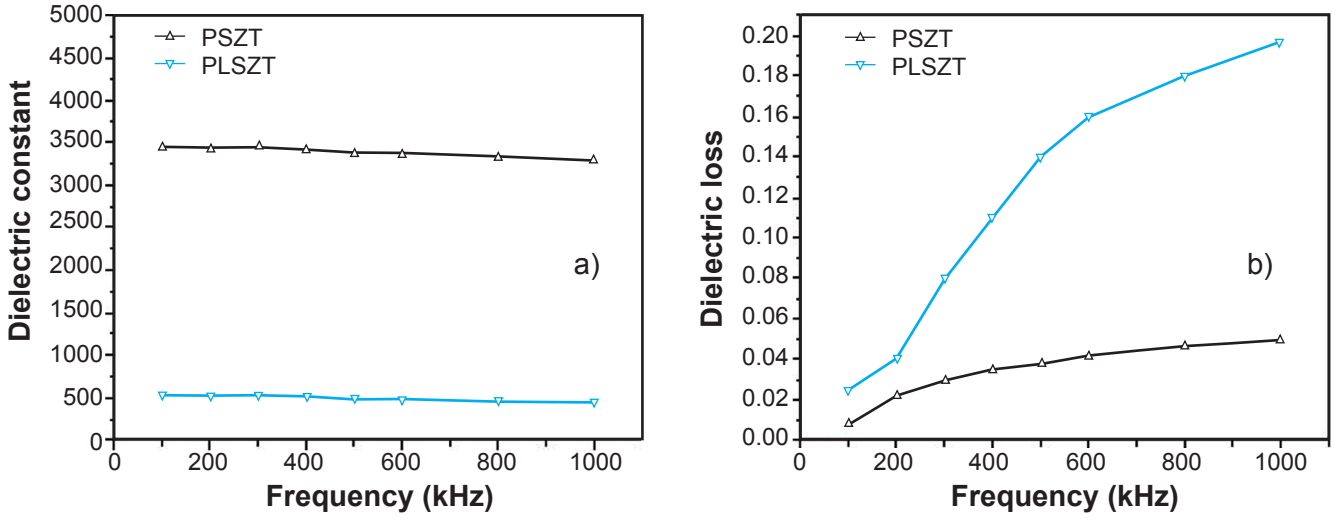

Figure 4: Frequency-dependence of dielectric constant (a) and dielectric loss (b) for soft and hard ceramics.

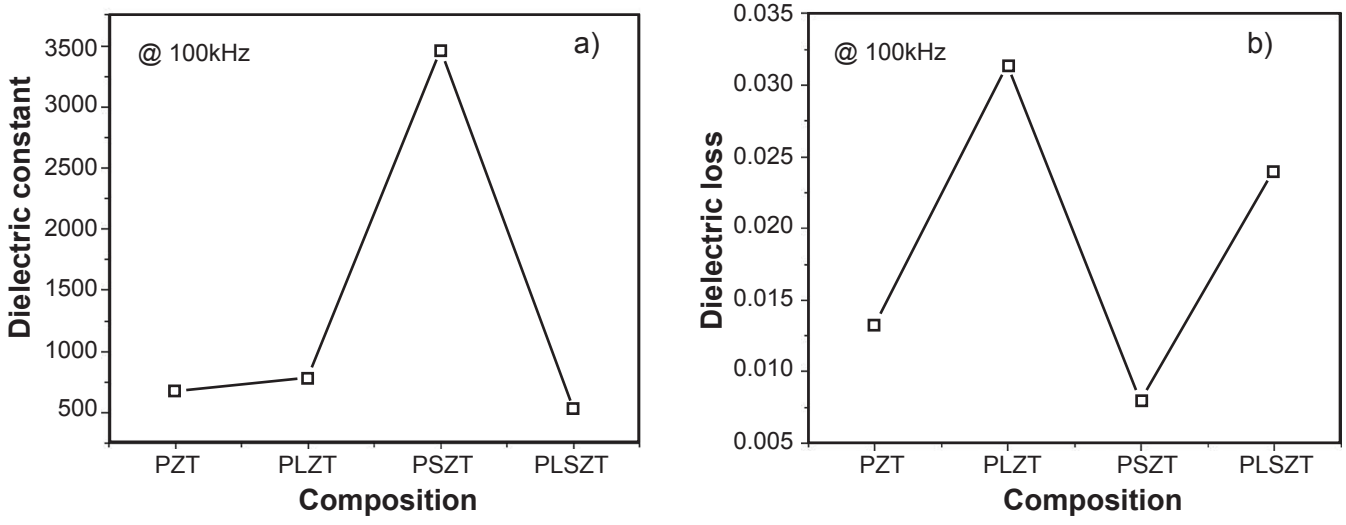

Figure 5: Influence of donor, acceptor, and complex doping on dielectric constant (a) and dielectric loss (b) of PZT ceramic.

both ceramics demonstrated dielectric constant value stability with frequency. However, the hard ceramic had higher values in comparison with those of ceramics with complex doping. Furthermore, both displayed a decrease in these values with increasing frequency. From 100 to 1000 kHz, ε_r values of PSZT and PLSZT ceramics decreased from 3450 to 3300 and from 525 to 430, respectively. This was owing to the effects of interfacial, orientation, and ionic polarization, which appeared completely where these dielectric constant values at low frequencies are particularly high. The reduction of ε_r values with increasing frequency can be explained as follow. The orientation of the polar group is relatively slow; this is because these consecutive polarizations cannot 'keep up' with the alternating field. The polarization direction cannot remain aligned with the field, and this polarization process no longer contributes to dielectric polarization. As a result, the values of the dielectric constant fall with increasing frequency, as is common in other insulators. On the other hand, Fig. 5 illustrates the effect of composition on the dielectric constant at 100 kHz and at room temperature. It was evident that the highest ε_r value was obtained in hard ceramic (PSZT) at around 3450. This can be ascribed to the relatively high porosity of the sample as can be seen from SEM images (Fig. 3), where it caused the increase in polarization which resulted from interstitial shipments at low frequencies.

Dielectric breakdown: the effect of the average rising voltage rate on the dielectric strength of hard and complex doped ceramics is presented in Fig. 6. With increasing voltage rate, both ceramics showed a progressive increase in dielectric strength values. Lower dielectric strength values with a slow voltage elevating rate of about 0.5 kV/s (i.e., long time) can be attributed to heat generation from leakage currents. It is well known that applying a voltage over an extended period of time increases the likelihood of an electrothermal breakdown since the increasing local temperature decreases the insulating properties of materials.

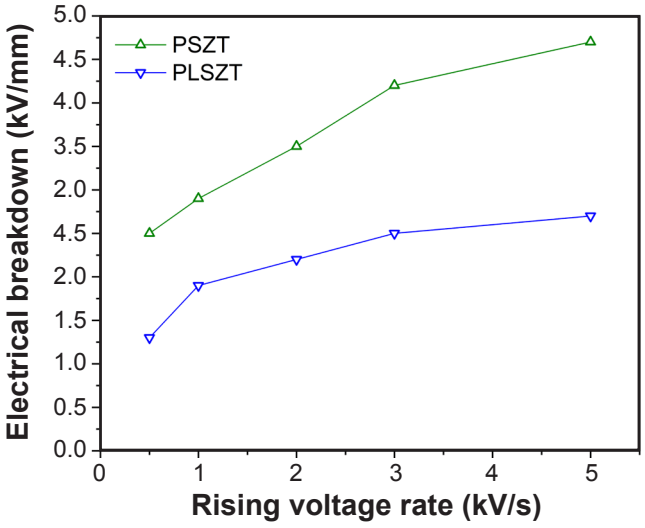

Figure 6: Dielectric strength versus average voltage elevating rate for hard and complex doped ceramics.

Furthermore, when materials are exposed to high voltage for an extended period of time, the cumulative effects of collision (chemical and electrochemical) and corrosion occur, destroying the materials and speeding up the breakdown by heating. On the other hand, higher values of dielectric strength were obtained at high voltage elevating rates, where an increase in this rate reduces the time required for two consecutive collisions of the same electron due to the acquisition of electrons to sufficient energy, speeding the process of ionization and thus speeding the breakdown, resulting in an increase in dielectric strength values. We saw irregularities in some areas of the overall behavior, and the cause was linked to faults in the bulk materials or homogenous weaknesses of each testing site in the sample [22-24].

Electrical conductivity: the influence of frequency on the electrical conductivity of soft and hard ceramics is illustrated in Fig. 7. Generally, the electrical conductivity changed linearly with frequency. This was due to the fact that at high frequency the capacitive reactance of the sample decreases, hence the impedance is reduced, which causes an increase in the ac conductivity of the sample.

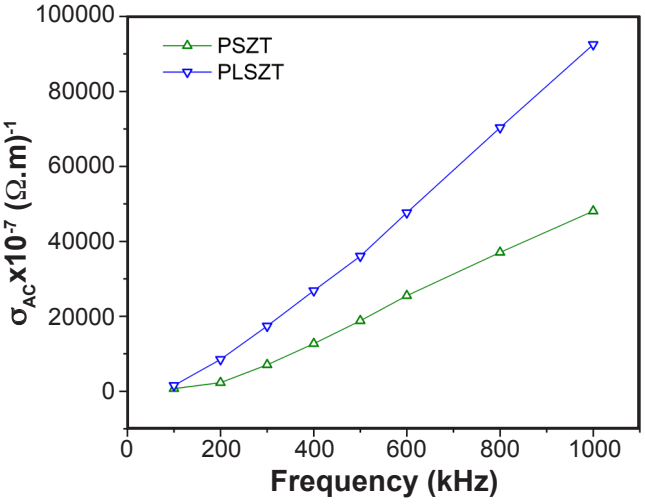

Figure 7: Electrical conductivity (σ_{AC}) as a function of frequency for soft and hard ceramics.

CONCLUSIONS

A PZT ceramic with a parent composition of $Pb_{1.03}(Zr_{0.56}Ti_{0.44})O_3$ characterized as rhombohedral structure according to the PZT phase diagram region was investigated systematically. Different strategies of doping were followed to investigate the influence of donor and acceptor ions in addition to complex doping on structural and microstructure properties of the parent composition: for the soft ceramic, 2 mol% lanthanum-doped PZT at A-site (PLZT), whereas 2 mol% of scandium-doped PZT at B-site to produce hard ceramic (PSZT). In terms of complex doping, 2 mol% of both La^{3+} and Sc^{3+} substituted A- and B-site, respectively (PLSZT). The ceramics were synthesized by solid-state

reaction. All samples showed dense and homogeneous microstructures, except PSZT ceramic which displayed a relatively small grain size. Previous studies showed that decreasing particle size improves dielectric breakdown strength (DBS), which in turn improves energy storage qualities. Therefore, it can be expected an increase in the energy storage values in the sample with complex doping as a result of grain size reduction. XRD results showed that the addition of Sc^{3+} induced phase transformation and formation of a coexistence region consisting of tetragonal and rhombohedral phases. This region was recognized in both PSZT and PLSZT compositions. Hard ceramic (Sc-doped PZT) exhibited the highest values of relative permittivity and lowest dielectric loss at a frequency of 100 kHz.

ACKNOWLEDGEMENT

The authors would like to thank the staff at the laboratories of the Department of Ceramic Engineering and Building Materials, College of Materials Engineering, University of Babylon, for their support in this work.

REFERENCES

[1] G.H. Haertling, J. Am. Ceram. Soc. **82**, 4 (1999) 797.
[2] L.L.W. Yang, Y.G. Wang, Y.J. Wang, X. Feng, Appl. Mech. Mater. **174-177** (2012) 592.
[3] L. Jin, "Broadband dielectric response in hard and soft PZT: understanding softening and hardening mechanisms", Ph.D. diss., Swiss Fed. Inst. Technol., Lausanne (2011).
[4] A. Zak, A. Jalalian, S. Hosseini, A. Kompany, T.S. Narm, Mater. Sci. Pol. **28**, 3 (2010) 703.
[5] J.D. Bobic, M.M.V. Petrovic, B.D. Stojanovic, in "Magnetic, ferroelectric, and multiferroic metal oxides", B.D. Stojanovic (Ed.), Elsevier (2018) 233.
[6] N. Zelikha, B. Ahmed, K. Amel, M. Hayet, B. Karima, A. Malika, A. Nora, M. Abdelhek, Int. J. Pharm. Chem. Biol. Sci. **4**, 3 (2014) 438.
[7] H.J. Lee, S.S. Won, K.H. Cho, C.K. Han, N. Mostovych, A.I. Kingon, S.-H. Kim, H.Y. Lee, Appl. Phys. Lett. **112**, 9 (2018) 92901.
[8] J. Xia, F. Cao, S. Yan, X. Chen, Z.-S. Lin, Y. Song, Y. Chen, X. Dong, G. Wang, AIP Adv. **10**, 9 (2020) 95132.
[9] M. Gao, X. Tang, S. Dai, J. Li, D. Viehland, Appl. Phys. Lett. **115**, 7 (2019) 72901.
[10] D. Mukherjee, M. Hordagoda, D. Pesquera, D. Ghosh, J.L. Jones, P. Mukherejee, S. Witanachchi, Phys. Rev. B **95**, 17 (2017) 174304.
[11] M.N. Al-Aaraji, "Nanostructured ferroelectric ceramics and coatings", PhD thesis, Univ. Manchester (2018).
[12] J.A.S. Caceres, C.A.C. Passos, J.V.S. Chagas, R.C. Barbieri, R.T. Corteletti, Mater. Res. **22**, 5 (2019) e20190123.
[13] S. Sangawar, B. Praveenkumar, P. Divya, H. Kumar, Mater. Today Proc. **2**, 4-5 (2015) 2789.
[14] D. Mahato, R. Chaudhary, S. Srivastava, J. Mater. Sci. Lett. **22**, 22 (2003) 1613.
[15] B. Mihailova, M. Gospodinov, B. Guttler, D. Petrova, R. Stosch, U. Bismayer, J. Phys. Condens. Matter **19**, 24 (2007) 246220.
[16] M. Correa, A. Kumar, R.S. Katiyar, Ferroelectrics **426**, 1 (2012) 112.
[17] M.K. Bhattarai, S.P. Pavunny, R.S. Katiyar, J. Appl. Phys. **130**, 3 (2021) 34103.
[18] M.K. Bhattarai, S.P. Pavunny, A.A. Instan, J.F. Scott, R.S. Katiyar, J. Appl. Phys. **121**, 19 (2017) 194102.
[19] L. Pdungsap, N. Udomkan, S. Boonyuen, P. Winotai, Sens. Actuator A Phys. **122**, 2 2005 (250).
[20] M. Hammer, M.J. Hoffmann, J. Electroceram. **2**, 2 (1998) 75.
[21] R.A. Langman, R.B. Runk, S.R. Butler, J. Am. Ceram. Soc. **56**, 9 (1973) 486.
[22] J. Kuffel, P. Kuffel, *High voltage engineering fundamentals*, Elsevier (2000).
[23] J.I. Kroschwitz (Ed.), "Electrical and electronic properties of polymers: a state-of-the-art compendium", Wiley-Interscience (1988).
[24] I. Bunget, M. Popescu, *Physics of solid dielectrics*, Elsevier, Amsterdam (1984).
(Rec. 13/11/2022, Rev. 12/03/2023, 07/05/2023, Ac. 15/05/2023)